Short crack propagation in LCF regime at room and high temperature in Q & T rotor steels

S. Rabbolini [a,*], S. Beretta [a], S. Foletti [a], A. Riva [b]

[a] Department of Mechanical Engineering, Politecnico di Milano, Via La Masa 1, Milan 20156, Italy
[b] Ansaldo Energia, Via Nicola Lorenzi 8, Genoa 16152, Italy

Received 17 August 2014
Received in revised form 5 January 2015
Accepted 9 January 2015
Available online 24 January 2015

1. Introduction

Fatigue life assessment in presence of defects (inclusions, inhomogeneities, ...) is important for massive components like rotors and disks of gas turbines, which are subjected to stress cycles induced by centrifugal loads and by differential temperatures during startups and shutdowns. The assessment is usually carried out by turbine manufacturers on isothermal LCF design curves [1].

Residual life of a component subjected to cyclic loading in Low Cycle Fatigue (LCF) regime can be assessed considering a crack propagating from the first load cycle, together with an appropriate crack growth model [2]. Traditional approach based on Linear Elastic Fracture Mechanics (LEFM) cannot be applied in LCF, since defects usually grow in zones where high plastic strains are present, such as near notches, violating LEFM main assumptions [3]. One way for describing crack growth rates in the LCF regime is to describe crack propagation as a function of the applied plastic strain range, $\Delta\epsilon_p$. The main contribution in this field is the work published by Tomkins [4], who related crack growth rates to the plastic strain range through an exponential law. Following these assumptions, Polak [5,6] was able to correctly estimate fatigue life of notched specimens, deriving model parameters from the traditional Manson–Coffin curve constants. A different formulation is the model proposed by Skelton [7], included in the British R5 procedure [8], who proposed a simplification by using more simply $\Delta\epsilon$ (for a given material $\Delta\epsilon_p = f(\Delta\epsilon)$). The Tomkins model, however, presents a limit, since it is able to correctly predict crack growth rate and fatigue life only when a marked plastic strain range is present, while unconservative estimates are obtained when the plastic part of the strain range tends to zero [9].

A different approach for describing crack growth rates in the LCF regime is the one based on the cyclic *J*-Integral, ΔJ. Dowling [10] extended Rice's path independent *J*-Integral [11] to the cyclic case, proposing to modify Paris relationship [12] by replacing the stress intensity factor range, ΔK, with ΔJ. Polak [13] was able to analyze the early propagation phase in an austenitic–ferritic duplex stainless steel by applying a ΔJ-based model, underlining the possibility to adopt cyclic *J*-integral models to describe short crack propagation. Härkegård [14] applied the *J*-Integral model to assess the fatigue life of specimens subjected to fully reversed strains in the LCF regime. In order to obtain conservative estimates, Harkegard considered a $da/dN - \Delta J$ curve estimated from crack propagation data at $R = 0$, in order to include the effects of crack closure.

* Corresponding author.
E-mail address: silvio.rabbolini@polimi.it (S. Rabbolini).

Nomenclature

a	crack length
a_0	initial crack length
a_f	crack length to failure
$c,\ m$	Paris Law constants
$g(n_i)$	function for plastic J-Integral range description
k_σ	McEvily model constant
k_i	cyclic strain/stress curve constant
n_i	cyclic strain/stress curve exponent
E	Young's modulus
R	strain ratio
Y	geometrical factor
ΔJ	J-Integral range
ΔJ_{eff}	effective J-Integral range
ΔK	stress intensity factor range
ΔW_e	elastic strain energy density
ΔW_p	plastic strain energy density
$\Delta\sigma$	stress range
$\Delta\sigma_{eff}$	effective stress range
$\Delta\epsilon$	strain range
$\Delta\epsilon_{eff}$	effective strain range
$\Delta\epsilon_e$	elastic strain range
$\Delta\epsilon_p$	plastic strain range
$\Delta\epsilon_{p,eff}$	effective plastic strain range
ϵ_a	strain amplitude
σ_{max}	maximum stress during the fatigue cycle
σ_a	stress amplitude
σ_{cl}	crack closing stress
σ_{open}	crack opening stress
$\sigma_{open,tr}$	transient crack opening stress

Apart approaches based on ΔJ, it has been recognized that plasticity induced crack closure plays an important role in LCF. Crack closure effects were implemented in ΔJ calculations by McClung and Sehitoglu [15,16] together with Seeger and Vormwald [17,18]. The reduction of the J-Integral range was quantified by lessening stress and plastic strain ranges, considering only the por-tion of the load cycle in which the crack stays open. Crack opening levels were calculated adopting the model proposed by Newman [19] for long cracks, where S_{op} for a given R depends on the con-straint factor and the ratio S_{max}/S_{flow}.

Lately, Zerbst et al. [20,21] proposed to apply the J-Integral calculation adopted in engineering fracture assessment [22,23]. In particular, from elastic stress intensity factor range, ΔJ is evaluated as a function of the yielding parameter $L_r = \sigma_{max}/\sigma_{ref}$ and then ΔJ_{eff} is calculated adopted the same concepts as Seeger & Vormwald. Another application of this model to short crack case and fatigue can be found in [24].

In this paper the application of ΔJ models to three different quenched and tempered CrMo rotor steels is discussed. In particular, an experimental campaign on micro-notched specimens at high temperature (up to 500 ° C) was developed. The results were examined in terms of crack growth rates and a series of cyclic ΔJ-Integral formulations were used to correlate these data with the external applied load. Experimental results showed that at high temperature there is a significant acceleration of short crack growth rates respect to crack growth models valid at room temper-ature because of the formation of a diffused damage ahead of the crack tip. This speed increment is temperature dependent.

2. Experiments

2.1. Test details

Fatigue crack growth behavior in LCF regime was investigated on three quenched and tempered CrMo steels adopted for manufacturing turbine disks and rotors. Steel #1, a bainitic steel, was tested at room temperature, since it is usually employed at low temperature, whereas steel #2 and steel #3 were tested at high temperature (490 and 500 °C respectively), because they are commonly used for turbine disks. Steel #2 is a different bainitic steel, whereas steel #3 is a ferritic–martensitic steel.

All LCF tests were performed using a MTS 810 servo-hydraulic testing machine. An high temperature longitudinal extensometer with a 12 mm long gage was employed and temperature was obtained with induction heating. In Fig. 1a, the experimental setup for high temperature testing is shown. LCF tests were carried out at a frequency of 0.5 Hz.

For each steel, two series of tests were carried out. In the first series, cylindrical specimens with a diameter of 8 mm and a gauge length of 20 mm were tested under constant strain amplitude loading at different amplitude levels, with a fixed strain ratio $R = -1$: Manson–Coffin curves were obtained from these datasets. In the second series, the same kind of tests were carried out on specimens containing artificial semicircular micro-notches, obtained by Electrical Discharge Machining (EDM): 400 μm depth notches were employed. Two additional experimental campaign were performed on steel #3 to confirm experimental observations. A new series of specimens, with an artificial defect of 100 μm, was tested at 350 °C with a fixed strain ratio $R = -1$. Another batch of specimens was tested at 500 °C with a fixed strain ratio $R = 0.25$ to check the influence of the applied mean strain on crack growth rates.

Crack propagation in LCF experiments was measured, after fatigue tests interruption, using the plastic replicas technique with a thin acetate foil. An example of a so-obtained replica at high temperature is presented in Fig. 1b, where, starting from the artificial defect, the surface crack propagation can be observed. An important assumption made during this analysis is that cracks maintain a semi-circular shape during propagation: this was confirmed during specimens inspection after the end of the tests, since the fracture surfaces of the broken specimens exhibited a semicircular fatigue crack. Experimental crack length was plotted against cycles: da/dN data were then derived by the *secant method* and models parameters calculation was based on these growth rate data.

In order to obtain reference $da/dN - \Delta K$ curves, a series of fatigue crack growth tests was performed on compact tension (C(T)) specimens. These experiments were carried out following the constant amplitude (CA) procedure proposed in the ASTM E647 standard. Initially, a stress ratio $R = 0$ was employed to evaluate the propagation curve necessary for Harkegard's model. A load ratio equal to 0.7 was then employed to obtain closure-free propagation curves. During all the experiments, the load frequency was fixed at 0.5 Hz, the same frequency adopted for LCF testing. A summary of the different series of experiments is shown in Table 1.

2.2. Strain life diagrams

All the experimental results at $R = -1$ are reported in Fig. 2a for steel #1, in Fig. 2b for steel #2 ($T = 490$ °C) and in Fig. 2c for steel #3 ($T = 500$ °C). Solid black dots represent tests performed on smooth specimens, whereas other data points show the results of

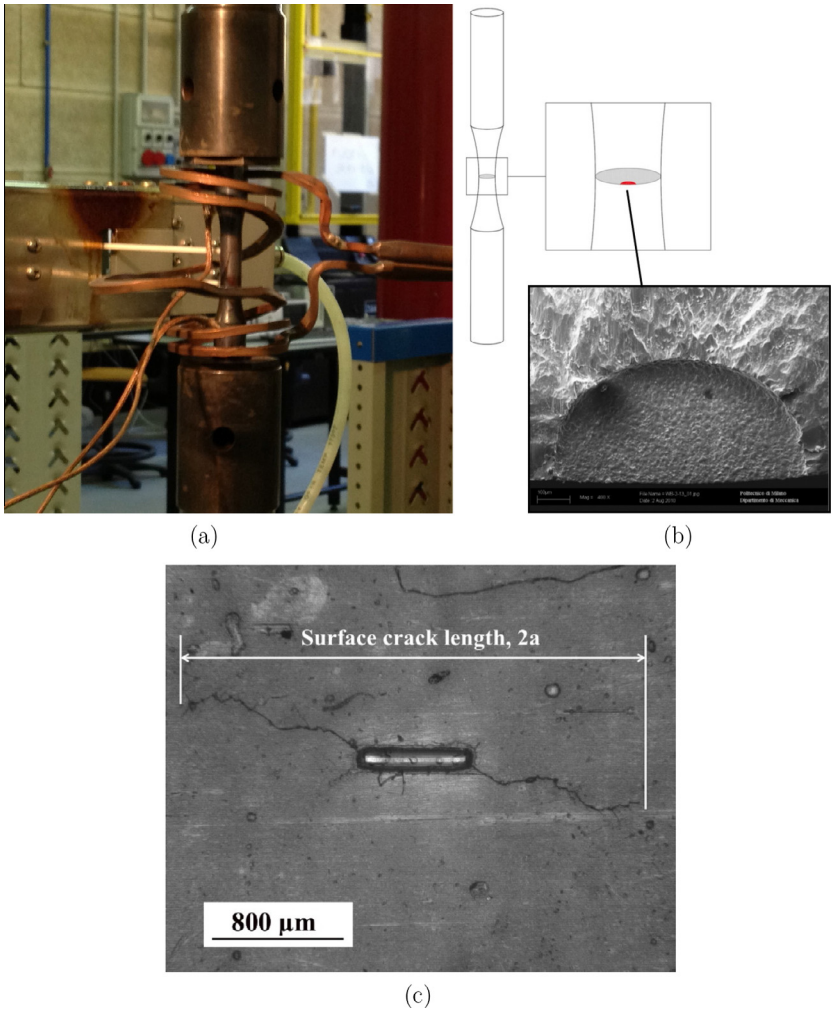

Fig. 1. LCF experimental tests: (a) experimental setup for HT LCF tests; (b) micro-notch shape and orientation (defect depth 400 µm); (c) surface crack propagation observed on a plastic replica, high temperature (defect depth 400 µm).

Table 1
Summary of the experimental tests.

Material	T (°C)	Test method	Test control	R
Steel #1	20	LCF – smooth specimens	Strain	−1
		LCF – specimens with 400 µm defects	Strain	−1
		FCG – C(T) specimens	Load	0–0.7
Steel #2	490	LCF – smooth specimens	Strain	−1
		LCF – specimens with 400 µm defects	Strain	−1
		FCG – C(T) specimens	Load	0–0.7
Steel #3	500	LCF – smooth specimens	Strain	−1
	500	LCF – specimens with 400 µm defects	Strain	−1
	500	LCF – specimens with 100 µm defects	Strain	0.25
	350	LCF – specimens with 100 µm defects	Strain	−1
	350–500	FCG – C(T) specimens	Load	0–0.7

tests conducted on micro-notched specimens. The number of cycles to fracture, N_f , is the number of cycles necessary to reach a load drop of 25%, corresponding to a final crack length $a_f = 3$ mm. Notched specimens were tested at four different strain levels, identified in Fig. 2a–c. Due to confidentiality issues, experi-mental results are presented in normalized form.

As it can be observed, micro-notches cause a marked drop in fatigue life, therefore it s a very important to have engineering tools for life assessment of engineering components. The different models for crack growth under LCFwill then be discussed in terms of their ability to predict the $\epsilon - N$ diagram for specimens with $a_o = 400$ µm.

3. Crack growth analysis

3.1. Cyclic J-Integral formulation

The cyclic J-Integral, ΔJ, can be described as the sum of an elastic and a plastic component [25]. The elastic part, considering plane strain conditions, can be calculated starting from LEFM [26]:

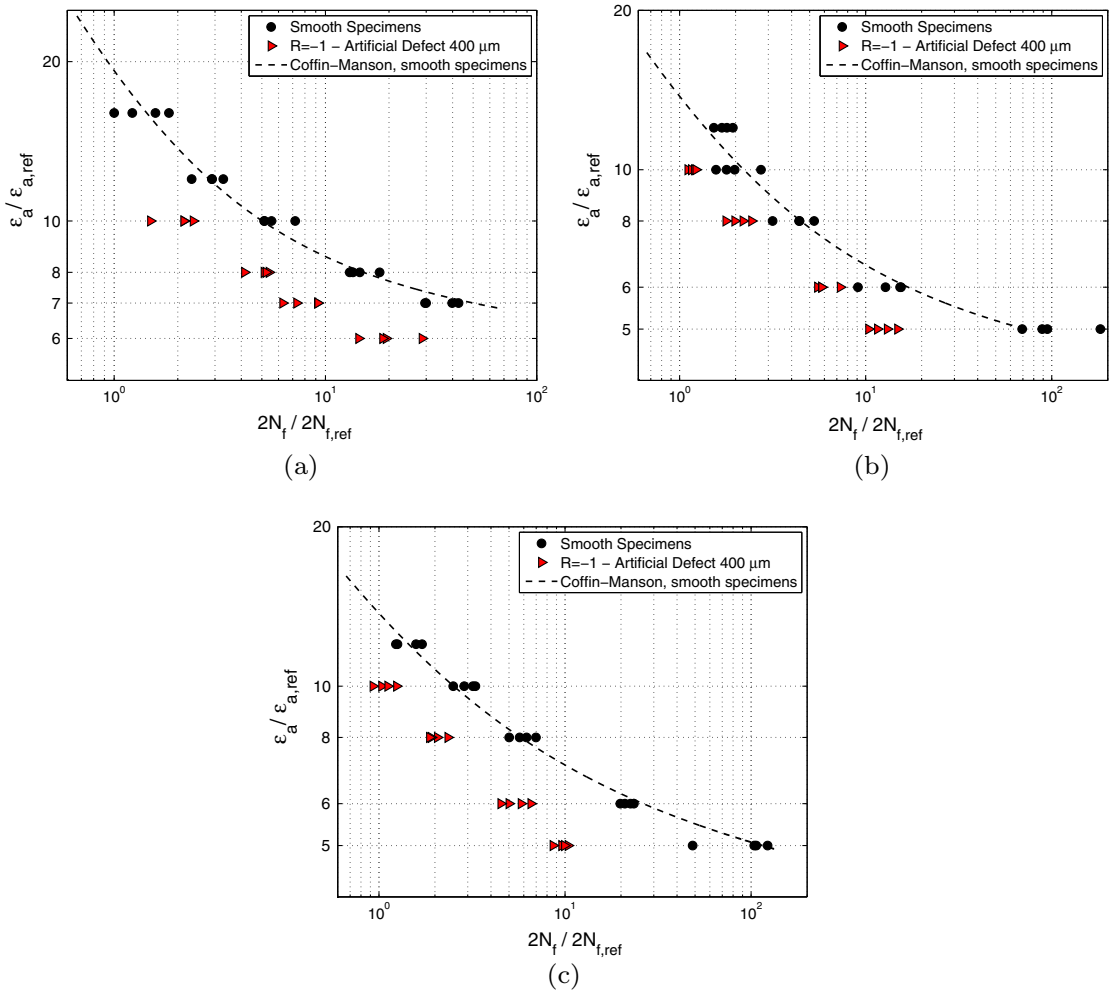

Fig. 2. Low Cycle Fatigue tests results. (a) Steel #1, room temperature; (b) steel #2, $T = 490$ °C; (c) steel #3, $T = 500$ °C.

$$\Delta J_e = \frac{\Delta K^2(1-\nu^2)}{E} = \frac{(Y\Delta\sigma\sqrt{\pi a})^2(1-\nu^2)}{E} = Y^2\frac{\Delta\sigma^2(1-\nu^2)}{E}\pi a = 2\pi Y^2(1-\nu^2)\Delta W_e a \quad (1)$$

where Y is a factor that accounts for crack geometry, a is the crack length, $\Delta\sigma$ is the applied stress range, E is the Young's modulus and ν is the Poisson's ratio. Consequently, ΔJ_e is a function of ΔW_e, the elastic strain energy density, evaluated as proposed in Eq. (2) and depicted in Fig. 3.

$$\Delta W_e = \frac{\Delta\sigma^2}{2E} \quad (2)$$

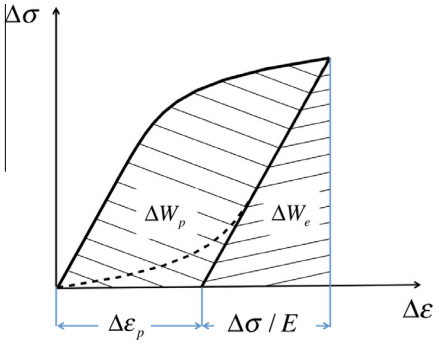

Fig. 3. Elastic and plastic strain energy density employed in ΔJ calculations.

The evaluation of the plastic part of the J-Integral range, ΔJ_p, follows the same path. Dowling postulated that ΔJ_p is proportional to ΔW_p, the plastic strain energy density [27], depicted in Fig. 3.

In these calculations, material plastic behavior is described by a pure power hardening law, as expressed in Eq. (3).

$$\Delta\epsilon = \frac{\Delta\sigma}{E} + 2\left(\frac{\Delta\sigma}{2k_i}\right)^{1/n_i} \quad (3)$$

Therefore, ΔW_P can be calculated as expressed in Eq. (4), where it is shown that the plastic strain energy density is a function of n_i, the hardening exponent, $\Delta\sigma$ and $\Delta\epsilon_p$, the plastic strain range.

$$\Delta W_p = \frac{\Delta\sigma\Delta\epsilon_p}{1+n_i} \quad (4)$$

Thus, ΔJ_p can be written as:

$$\Delta J_p = 2\pi Y^2 f(n_i)\Delta W_p a \quad (5)$$

where $f(n_i)$ is a function that takes into account crack geometry and material elastic–plastic behavior. Several formulations of $f(n_i)$ are proposed in [25] and in [28]. Following these observations, the general formulation of ΔJ can be written as:

$$\Delta J = \Delta J_e + \Delta J_p = 2\pi Y^2 a\left[(1-\nu^2)\Delta W_e + f(n_i)\Delta W_p\right] \quad (6)$$

Eq. (6) shows that ΔJ is a function of both elastic and plastic strain energy density, a feature that makes the J-Integral range a parameter capable of measuring the characteristic crack-tip strain field.

This means that, in elastic–plastic fracture mechanics, ΔJ can play the same role of the stress intensity factor range, ΔK, in LEFM [27]. Moreover, following this description, ΔJ can be computed directly from the hysteresis loops, by fitting the upper branch of the stress/strain fatigue cycle with the Ramberg–Osgood equation, as shown in Fig. 3. This definition is in line with the Z – *integral* con-cept presented in [29].

The ΔJ formulations proposed by Polak [13] and Härkegård [14] are here reported. For the given geometry, Polak modified Eq. (6), proposing the formulation:

$$\Delta J = \frac{\Delta K^2}{E} + 1.72 g(n_i)\sigma_a \epsilon_a a \tag{7}$$

where σ_a and ϵ_a are stress and strain amplitudes, ΔK is the stress intensity factor range and $g(n_i)$ is evaluated as [28]:

$$g(n_i) = (1 - n_i)\left(3.85\sqrt{\frac{1}{n_i}}(1 - n_i) - \pi n_i\right) \tag{8}$$

Even Harkegard's formulation is derived directly from Eq. (6) and, for the given geometry, is expressed as:

$$\Delta J = Y^2 \pi a \Delta\sigma\left(\Delta\epsilon_e + 2\Delta\epsilon_p\right) \tag{9}$$

3.2. Effective cyclic J-Integral formulation

Starting from Dowling's proposal [10], effective elastic–plastic J-Integral range for the given geometry can be evaluated as [17]:

$$\Delta J_{eff} = a\left[1.24\frac{\Delta\sigma_{eff}^2}{E} + \frac{1.02}{\sqrt{n_i}}\Delta\sigma_{eff}\Delta\epsilon_{p,eff}\right] \tag{10}$$

where a is crack length, E is Young's modulus, n' is the exponent of the cyclic stress–strain curve, $\Delta\sigma_{eff}$ and $\Delta\epsilon_{p,eff}$ are, respectively, the effective stress range and the effective plastic strain range. $\Delta\epsilon_{p,eff}$ is calculated as:

$$\Delta\epsilon_{p,eff} = \Delta\epsilon_{eff} - \frac{\Delta\sigma_{eff}}{E} \tag{11}$$

The effects of crack closure in ΔJ evaluation are related to the calculation of crack opening and closing stresses. In the model proposed by Vormwald and Seeger [17], crack opening stress, σ_{open}, is calculated from Newman's equations [19]. Experimental results, reported in [17,15], showed that, during LCF propagation, a satisfactory estimate of crack opening levels can be obtained by considering plane stress (i.e. $\alpha = 1$), since significant out-of-plane constraint is less likely under general yielding [15]. The cyclic flow stress, a parameter necessary for the calculation of crack opening stress in Newman's model, is estimated as the average of the cyclic yield stress and the ultimate strength [30].

It has ben shown [17], that, during short crack propagation, crack closing occurs at the same strain level registered at opening. Therefore, according to this model, σ_{cl}, the crack closing stress, is lower than σ_{open}. This implies that, according to Vormwald and Seeger, the effective stress range should be calculated as proposed in Eq. (12):

$$\Delta\sigma_{eff} = \sigma_{max} - \sigma_{cl} \tag{12}$$

where σ_{max} is the stress peak value and σ_{cl} is crack closing stress. A summary of the significant points of Vormald and Seeger's model is depicted in Fig. 4, in which the hatched area represents the part of the hysteresis loop considered for ΔJ computation, according to Dowling [31].

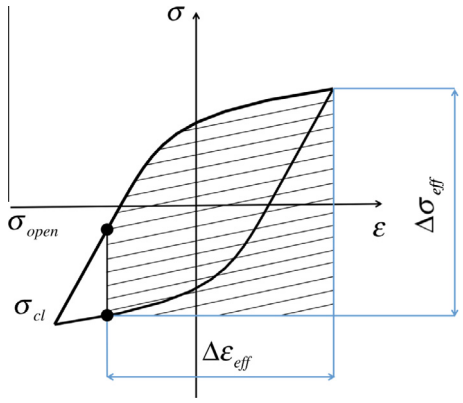

Fig. 4. Definition of the significant part of the stress/strain cycle according to Vormwald and Seeger [17].

3.3. Data analysis and comparison of the models

All the experimental datas were analyzed considering experimental stresses and strains extracted from the stabilized stress/strain loop, taken at $N_f/2$. The upper branch of the fatigue load cycle was fitted with the Ramberg–Osgood equation proposed in Fig. 3: this allowed the direct estimation of ΔJ from the hysteresis loops, following Dowling's initial proposal.

The different models have then been compared in terms of description of the estimated $da/dN - \Delta J$ (or $da/dN - \Delta J_{eff}$ data) and their ability to predict the $\epsilon - N$ diagram for specimens with defects. In particular, for the differently estimated da/dN curves, life prediction for micronotched specimens have then been calculated as:

$$N_f = \int_{a_o}^{a_f} \frac{1}{da/dN} da \tag{13}$$

assuming $a_o = 400$ μm (cracks grew from the micronotches almost from the first load cycle) and $a_f = 3$ mm (average crack depth for the broken specimens).

4. Results and discussion

4.1. LCF tests at RT

In Fig. 5a experimental results are reported in terms of crack growth rates for steel #1, considering Polak's formulation (Eq. (7)). This model introduces a large scatter, a feature present even when Harkegard's formulation (Eq. (9)) is considered (Fig. 5b): this is due to the fact that models based on the cyclic J-Integral range neglect the effects of crack closure during propagation.

The experimental points, obtained considering Polak's and Harkegard's formulations, can be fitted by a modified Paris law (Eq. (14)):

$$\frac{da}{dN} = c \cdot \Delta J^m \tag{14}$$

where c and m parameters were estimated by a least squares interpolation of experimental data points. Fatigue life was estimated from Eq. (13) adopting these parameters. The results in terms of fatigue life prediction, obtained considering Polak's formulation, are represented in Fig. 5d by a light grey line: the scatter observed in Fig. 5a is responsible for the unconservative assessment, in particular for those tests performed at high strain ranges whose experimental growth rate data are higher than the average $da/dN - \Delta J$ curve.

Much better results could be obtained with Harkegard's model. In details, in order to obtain conservative estimates, the author [14]

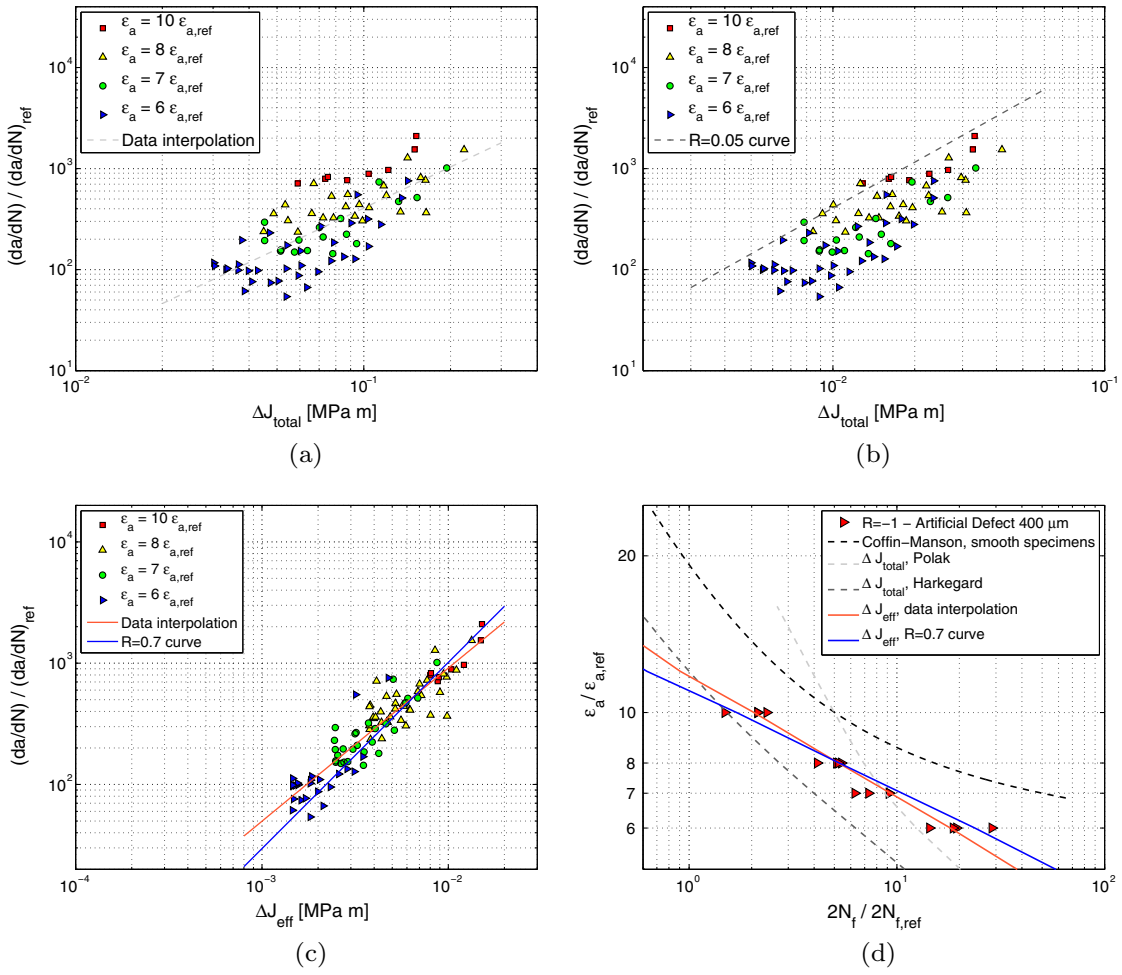

Fig. 5. Fatigue crack growth analysis for steel #1, room temperature: (a) Crack growth rates vs. ΔJ_{tot} according to Polak; (b) crack growth rates vs. ΔJ_{tot} according to Harkegard; (c) crack growth rates vs. ΔJ_{eff}; (d) fatigue life prediction for micronotched specimens ($a_o = 400$ μm).

suggested to consider the crack propagation curve obtained testing fracture specimens at $R = 0$ (the dark grey line in Fig. 5b). As it can be seen, this propagation curve is an upper bound for the experimental data-points. This means that a fatigue life prediction based on Harkegard's formulation (the dark grey line in Fig. 5d) is conservative for all the considered strain ranges. Such an approach, however, provides very conservative results (in a factor 3) at low strain levels.

Finally, crack propagation model based on Eq. (10) was implemented. The model was modified to take into account that, in the early propagation stage, cracks are open even at minimum load. This phenomenon, observed in [15], is due to the transient build-up of crack-closure and can be implemented by considering the model by McEvily [32] as proposed in [24]. This model describes crack opening load, as dependent on crack advance as:

$$\sigma_{open,tr} = \sigma_{min} + (\sigma_{open} - \sigma_{min})\{1 - exp[-k_{op}(a - a_o)]\} \qquad (15)$$

where k_{op} is a material dependent constant and a_o is initial notch size. This parameter was estimated interpolating experimental data and it has resulted to be close to the value obtained in [24].

Final results for steel #1 in terms of crack growth rates, obtained considering ΔJ_{eff} (Eq. (10)), are reported in Fig. 5c: experimental points tend to align to a single line and a much smaller scatter is observed. In the same picture, experimental data were compared with the trend line from $da/dN - \Delta K_{eff}$ data obtained on C(T) specimens at high load ratio ($R = 0.7$). As it can be seen, experimental data are very close to $da/dN - \Delta K_{eff}$ curve: this is due to the fact that Vormwald and Seeger's model considers and removes crack closure effects. It is worth remarking that the predicted $\epsilon - N$ curve for micronotched specimens, due to improvement offered by Eq. (15), is very close to experimental results (both considering $da/dN - \Delta J_{eff}$ average interpolation or $da/dN - \Delta K_{eff}$ curve) also at very low strain amplitudes where $\Delta\epsilon_p$ becomes negligible. This means that ΔJ_{eff} model is able to describe well the life also in the region, very interesting for engineering applications like turbines whose target life is 10,000–20,000 cycles, where Tomkin's model provides unconservative estimates, as discussed in [9].

4.2. LCF tests at HT

Experimental results obtained at HT will be discussed considering the $\Delta - J_{eff}$ model since it has proven to be very precise. Experimental results for steel #2 and #3 are shown in Figs. 6 and 7. At high temperature, fatigue crack growth rates measured in notched specimens do not match with those observed in C(T) testing, as shown in Figs. 6a and 7a. A marked speed increment is evident, meaning that fatigue life prediction based on $da/dN - \Delta K_{eff}$ curves can lead to unconservative results, as depicted in Figs. 6b and 7b.

The presence of the speed increment was confirmed even by the tests performed at $R = 0.25$ on steel #3 at 500 °C: as it can be seen in Fig. 8a, experimental data points, obtained testing specimens with an applied mean strain, lie on the same line of those tested at $R = -1$. This confirms the enhanced crack growth at 500 °C.

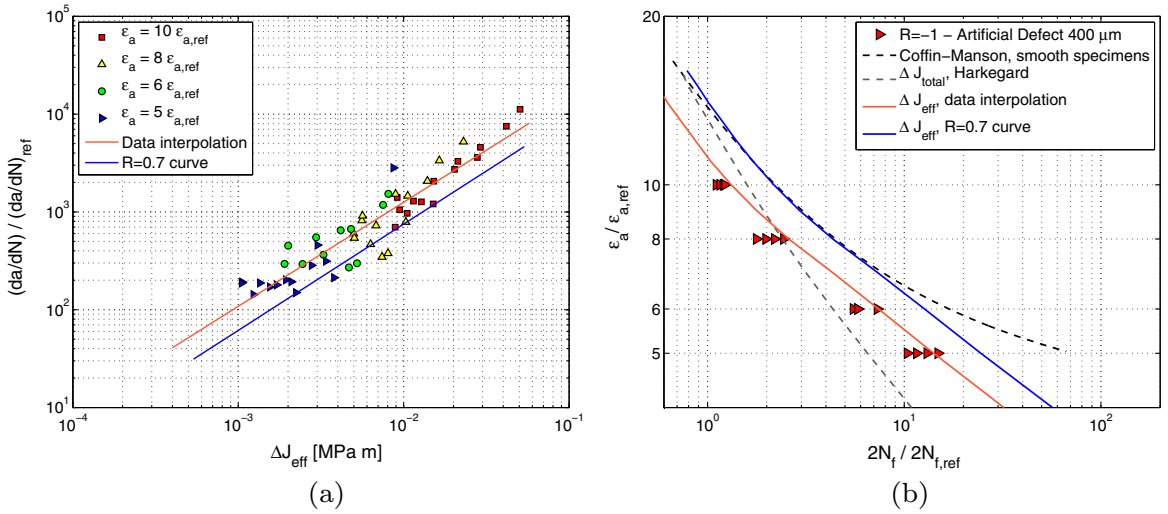

Fig. 6. Fatigue crack growth analysis for steel #2, $T = 490$ °C. (a) Crack growth rates against effective J-Integral range; (b) fatigue life prediction.

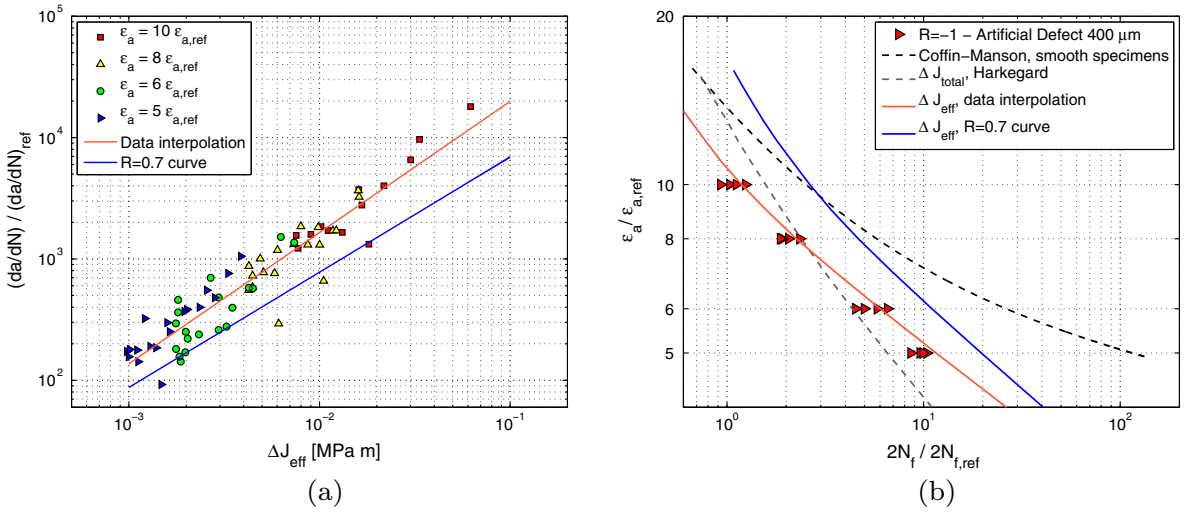

Fig. 7. Fatigue crack growth analysis for steel #3, $T = 500$ °C. (a) Crack growth rates against effective J-Integral range; (b) fatigue life prediction.

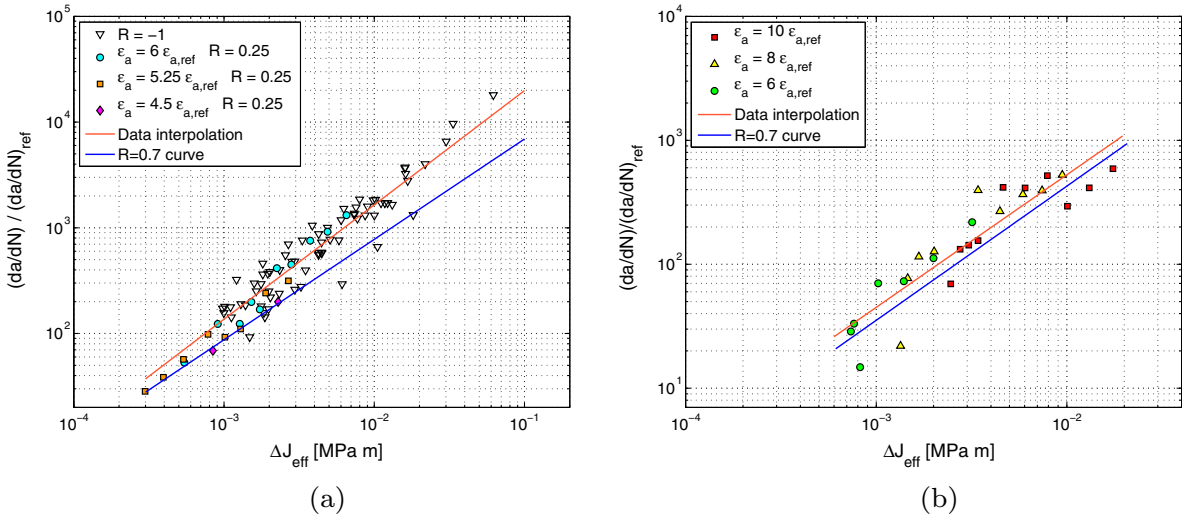

Fig. 8. Additional tests for steel #3: (a) tests at $R = 0.25$, $T = 500$ °C; (b) tests at $R = -1$, $T = 350$ °C.

Another series of tests at 350 °C were carried out on steel #3, in order to check a possible temperature dependence of the crack growth rates increment. Results for the new series are shown as it can be observed in Fig. 8b: the $da/dN - \Delta J_{eff}$ data are only slightly higher than the ΔK_{eff} curve, but the growth enhancement tends to disappear and it is much lower than the scatter of the data.

The fact that at high levels of ΔJ the growth rate of small cracks is higher than the one of long cracks was already noted by Earthman [33] in LCF tests similar to the present results (steel similar to #3 tested at 600 °C), who attributed it to an increased contribu-tion of plastic deformation at the crack tip. Fractographic analyses of crack surface give a more robust explanation for the registered speed increment: in Fig. 9, a comparison between low temperature (350 °C) and high temperature (500 °C) fracture for steel #3 is shown. As it can be seen, at 500 °C several micro-cracks are present, propagating from defect main body. Moreover, at high temperature, the material presents a damaged area ahead of the crack tip, meaning that, at high temperature, the material is damaged even before crack propagation. The shape of the fracture surface at 500 °C shows that the crack does not follow a straight pattern, but propagates in weak regions at grain boundaries for steel #3 [34]. Crack growth rates increment is then significant at 500 °C because of this damage mechanism ahead of the crack tip: this pos-sibly explains why the enhanced growth rate is temperature dependent. Oppositely, experiments on long cracks for a steel with the same composition as #3 [35] have shown that crack surface oxidization at high temperature tends to increase the closure level (respect to an inert atmosfere) and to increase ΔK_{th}.

Fractographic observations confirmed a similar damage mechanism also for steel #2, as shown in Fig. 9c, even though the patterns of microcracking looks to be different.

It is of some importance also to remark that Harkegard's model, which usually provides conservative results (see Fig. 5d), underestimates the life at the higher strain amplitudes both for steel #2 and steel #3 (see dashed grey line in Figs. 6b and 7b). This confirms the systematic crack growth acceleration at evidenced by the $da/dN - \Delta J_{eff}$ graphs and the need of incorporating this *enhanced short crack growth* into life prediction.

4.3. Correction of growth rate for damage at the crack tip

Summarizing results on steel #3, an average speed factor s_f could be expressed as:

$$s_f = \frac{(da/dN)_{exp}}{(da/dN)_{R=0.7}} \tag{16}$$

where da/dN_{exp} is the experimental growth rate and $da/dN_{R=0.7}$ is the growth obtained from long crack at $R = 0.7$. In particular data were interpolated with Eq. (14) power law and the s_f factor was evaluated on the interpolating curve at the mean value of ΔJ_{eff} range (its scatter was similarly evaluated from 5% to 95% percentiles of the experimental data). The s_f factor is shown in Fig. 10, where it is clear that the enhanced growth rate can be neglected for temperatures below 300 °C (the scatter at RT was taken from data of *steel* #1).

The meaning of this speed factor is that, for a correct life estimation based onto ΔJ_{eff}, the growth rate *effective curve* (the $da/dN - \Delta K_{eff}$ curve) should be multiplied by s_f. As a further support to the present results, a similar trend for s_f factor was also obtained with the ΔJ_{eff} formulations proposed by Sehitoglu and McClung and by Zerbst et al. (see [36], details are not presented here for the sake of brevity).

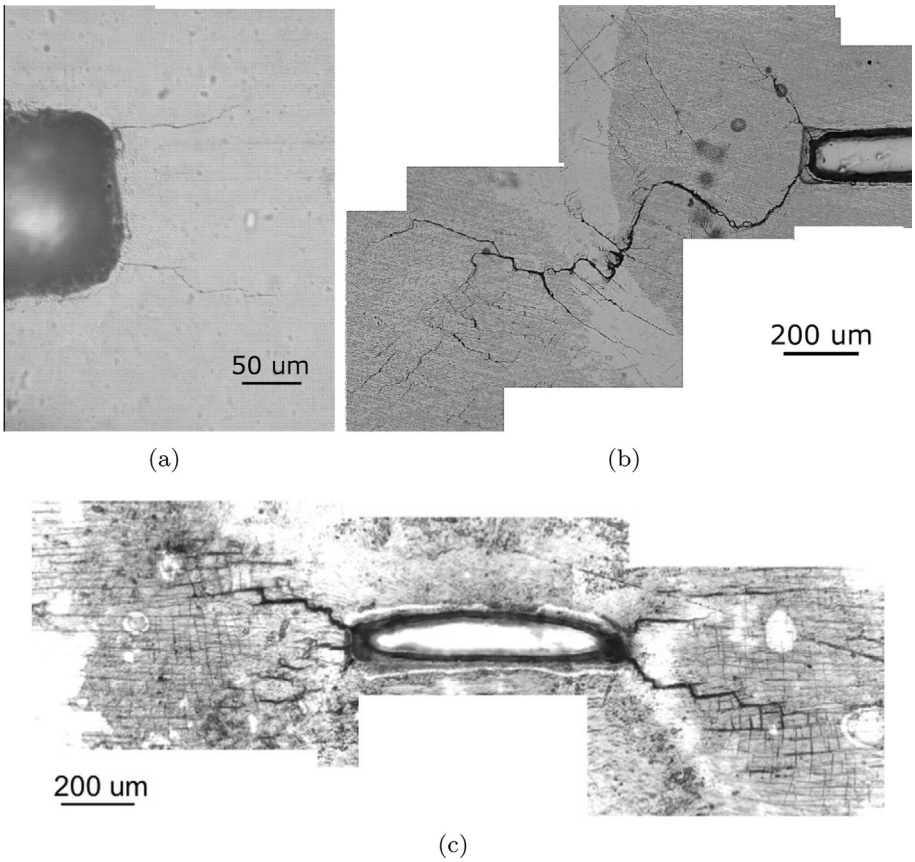

Fig. 9. Comparison between fracture surfaces at different temperatures, steel #2 and #3. (a) Steel # 3, $T = 350$ °C; (b) steel # 3, $T = 500$ °C; (b) steel # 2, $T = 490$ °C.

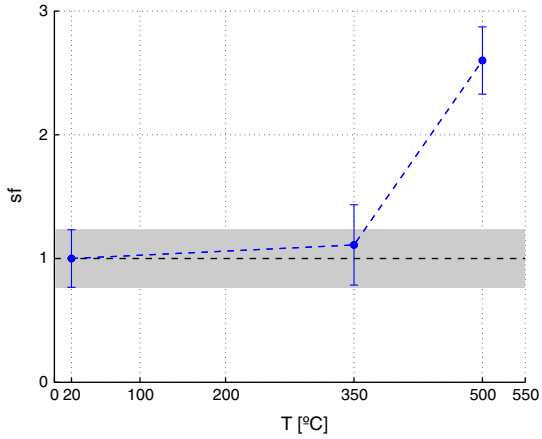

Fig. 10. Speed increment factor against testing temperature together with 90% scatter band (5–95% percentiles): the grey area corresponds to the scatter evaluated at RT for steel #1.

5. Conclusions

In this paper we have investigated the methods for predicting LCF fatigue life in presence of micro-defects for three Q & T CrMo rotor steels. LCF tests at different temperatures were carried out on different cylindrical specimens: smooth samples were employed for Coffin–Manson curve evaluation, whereas notched specimens were used to measure crack growth rate.

Three different Elastic–Plastic J-Integral models (two based onto ΔJ and another one onto ΔJ_{eff}) were implemented and checked against experimental crack growth rates and predictions of the $\epsilon - N$ diagram. The $da/dN - \Delta J$ data obtained with the formulation proposed by Polak were affected by a large scatter. This scatter was then responsible for inaccurate fatigue life predictions, in particular when high plastic strains were applied. Even Harkegard's model provided scattered data, but the proposed growth curve (obtained from $da/dN - \Delta K$ data at $R = 0$) gave a conservative description of the growth rate. In terms of $\epsilon - N$ diagram, such an approach provided conservative results, especially at low strain amplitudes.

Taking into account crack-closure effects, Vormwald and Seeger's ΔJ_{eff} model was able to condense the growth rate onto a single $da/dN - \Delta J_{eff}$ curve. At room temperature this propagation curve matched with the one obtained from tests conducted on compact tension specimens at $R = 0.7$. At high temperature a marked speed increment was observed. An accurate analysis of the fracture surfaces showed that a peculiar damage mechanism, which consists of a diffuse cracking ahead of the crack tip, was present at high temperature. The phenomenon was temperature dependent, since experimental tests performed at lower temperatures did not show the same damage mechanism. The presence of this damage ahead of short cracks makes it necessary to adopt a suitable crack growth rate correction factor, otherwise the models would provide unconservative life estimates at high temperature.

Acknowledgments

The present research has been developed in the frame of a technical cooperation between Politecnico di Milano, Dept. Mechanical Engineering, and Ansaldo Energia Spa -AEN (Genova, Italy) about methods for life prediction of turbine components.

References

[1] Muehle E, Ewald J. High-reliability steam turbine components – material and strength calculation aspects. In: High temperature materials for power engineering. Dordrecht: Kluwer Academic Publishers; 1990.
[2] Miller K, Murakami Y. What is fatigue damage? A view point from the observation of low cycle fatigue process. Int J Fatigue 2005;27(8):991–1005.
[3] Miller K. Materials science perspective of metal fatigue resistance. Mater Sci Technol 1993;9(6):453–62.
[4] Tomkins B. Fatigue crack propagation – an analysis. Philos Mag 1968;18(155):1041.
[5] Polak J. Plastic strain-controlled short crack growth and fatigue life. Int J Fatigue 2005;27:1192–201.
[6] Polak J, Kruml T, Obrtlik K, Man J, Petrenec M. Short crack growth in polycrystalline materials. Procedia Eng 2010;2:883–92.
[7] Skelton R. The prediction of crack growth rates from total endurances in high strain fatigue – thirty years on. Fatigue Fract Eng Mater Struct 2008;32(2):81–3.
[8] Assessment procedure R5. British Energy Generation Ltd.; 2003.
[9] Beretta S, Foletti S, Rabbolini S, Bordo LE, Sanguineti A, Traversone L. Models for small crack growth in LCF at room temperature and high temperature. In: ASME turbo expo 2012: turbine technical conference and exposition. American Society of Mechanical Engineers; 2012. p. 323–30.
[10] Dowling N. Cyclic stress–strain and plastic deformation aspects of fatigue crack growth. ASTM; 1977.
[11] Rice J. A path independent integral and the approximate analysis of strain concentration. J Appl Mech 1968;35:379–86.
[12] Paris P, Erdogan F. A critical analysis of crack propagation laws. Basic Eng Trans ASME Ser D 1963;85:528–34.
[13] Zezulka P, Polak J. Short crack growth and fatigue life in austenitic–ferritic duplex stainless steel. Fatigue Fract Eng Mater Struct 2005;28(10):923–35.
[14] Härkegård G, Denk J, Stärk K. Growth of naturally initiated fatigue cracks in ferritic gas turbine rotor steels. Int J Fatigue 2005;27(6):715–26.
[15] McClung R, Sehitoglu H. Closure behavior of small cracks under high strain fatigue histories. In: Newman J, Elber W, editors. Mechanics of fatigue crack closure. ASTM; 1988. p. 279–99 [chapter 2].
[16] McClung R, Sehitoglu H. Characterization of fatigue crack growth in intermediate and large scale yielding. J Eng Mater Technol 1991;113:15–22.
[17] Vormwald M, Seeger T. The consequences of short crack closure on fatigue crack growth under variable amplitude loading. Fatigue Fract Eng Mater Struct 1991;14(2/3):205–25.
[18] Radaj D, Vormwald M. Elastic–plastic fatigue crack growth. In: Advanced methods of fatigue assessment. Springer; 2013. p. 391–481.
[19] Newman J. A crack-closure model for predicting fatigue crack growth under aircraft spectrum loading. In: Chang J, Hudson C, editors. Methods and models for predicting fatigue crack growth under random loading. ASTM; 1981. p. 53–84.
[20] Zerbst U, Madia M, Hellmann D. An analytical fracture mechanics model for estimation of s-n curves of metallic alloys containing large second phase particles. Eng Fract Mech 2012;82:115–34.
[21] Zerbst U, Madia M, Eufinger J, Bruder T. Bruchmechanisches modell zur ermittlung der schwingfestigkeit von geschweißten und nichtgeschweißten proben. Mater Test 2013;55(7–8):511–9. http://dx.doi.org/10.3139/120.110465.
[22] R6. Assessment of the integrity of structures containing defects. British Energy Generation Ltd.; 2000.
[23] Zerbst U, Schodel M, Webster S, Ainsworth R. Fitness-for-Service fracture assessment of structures containing cracks. A workbook based on the European SINTAP/FITNET procedure. Elsevier Science; 2007.
[24] Eufinger J, Heinrietz A, Bruder T, Hanselka H. An engineering approach to fatigue analysis based on elastic–plastic fracture mechanics. Fatigue Fract Eng Mater Struct 2013;36(1):65–74.
[25] Dowling N. J-integral estimates for cracks in infinite bodies. Eng Fract Mech 1987;26(3):333–48.
[26] Paris P, Sih G. Stress analysis of cracks. In: Fracture toughness testing and its applications. ASTM; 1965. p. 30–83.
[27] Dowling N. Crack growth during low-cycle fatigue of smooth axial specimens. ASTM Stp 1977;637:97–121.
[28] Shih C, Hutchinson J. Fully plastic solutions and large scale yielding estimates for plane stress crack problems. J Eng Mater Technol 1976;98:289–95.
[29] Wüthrich C. The extension of the J-integral concept to fatigue cracks. Int J Fract 1982;20(2):R35–7.
[30] Vormwald M. Crack initiation life prediction based on fracture mechanics for short cracks. Ph.D. thesis. Technical University Darmstadt; 1989.
[31] Dowling N, Begley J. Fatigue crack growth during gross plasticity and the J-integral. In: Mechanics of crack growth. ASTM; 1976. p. 82–103.
[32] McEvily A, Endo M, Murakami Y. On the area relationship and the short fatigue crack threshold. Fatigue Fract Eng Mater Struct 2003;26:269–78.
[33] Earthman J. Characterization of small crack growth in 12% CrMoV steel under high temperature, low cycle fatigue conditions. Mater Sci Eng 1991;A132:89–95.
[34] Jara DR. 9–12% Cr heat resistant steels: alloy design, TEM characterisation of microstructure evolution and creep response at 650 ° c. Ph.D. thesis. Ruhr-Universitat Bochum; 2011.
[35] Lee J-H, Kim B-J, Kim MK, Lim B-S. Effects of temperature and oxidation on threshold stress intensity factor of 12% Cr steel for steam turbine rotor component. J Mech Sci Technol 2013;27(5):1273–7.
[36] Rabbolini S. Methods for LCF life predictions in presence of defects. Ph.D. thesis. Milano: Politecnico di Milano; 2014.